Available online at www.sciencedirect.com
SCIENCE DIRECT®
European Journal of Mechanics B/Fluids 23 (2004) 65–80

From the double vortex street behind a cylinder to the wake of a sphere

Michel Provansal, Lionel Schouveiler, Thomas Leweke *

Institut de recherche sur les phénomènes hors equilibre, UMR 6594 CNRS/Universités Aix-Marseille, technopôle de Château-Gombert, 49, rue Frédéric Joliot Curie, BP 146, 13384 Marseille cedex 13, France

Received 11 July 2003; received in revised form 18 September 2003; accepted 19 September 2003

Abstract

In this paper, we review the main results concerning the first instabilities, characterised by the breaking of spatio–temporal symmetries, occurring in the wake of bluff bodies, as the flow speed is increased. Phenomenological wake models are compared to experiments for the geometry of a circular cylinder and of a sphere. The transition from a cylindrical to spherical configuration is also illustrated in various ways, such as the transverse coupling of two sphere wakes and a reduction in length or a wavy deformation of a circular cylinder. Finally, we report preliminary results concerning the fluid–structure interactions in the case of a longitudinally tethered sphere.

Keywords: Circular cylinder wake; Sphere wake; Landau and Ginzburg–Landau models; Fluid–structure interaction

1. Introduction

The formation and dynamics of the Bénard–von Kármán vortex street [1,2] behind a circular cylinder have been the subject of several hundred publications (see the different reviews in [3–7]). This very large number is linked to the importance of this type of flow for applications in different engineering fields and to the apparent simplicity of this configuration. Surprisingly, measurements of the amplitudes of wake oscillations and the careful analysis of the spatial structure of the vortex shedding characterising this instability, including the associated phase lines, have only been undertaken a long time after the discovery of the phenomenon and the initial theoretical study of the stability of an ideal alternating vortex street by von Kármán [2]. In the absence of an analytical description of this flow, phenomenological models like the one presented below, which are able to capture essential features of the flow dynamics and bifurcations at low Reynolds numbers, have proven to be very helpful in this respect.

After a short presentation of the Landau wake model in Section 2, we present in Section 3 a comparison between experimental observations and predictions of this model, obtained analytically and numerically, for vortex shedding behind a cylinder. The Ginzburg–Landau model is an extension of the Landau model, which can account for the main three-dimensional aspects of vortex shedding. Section 4 is devoted to the comparison of the Landau model with the wake characteristics of a single sphere. The numerical values of the parameters of the model are determined in the same way as in the case of the cylinder. In addition to the laminar case, the variation of the vortex shedding frequency with Reynolds number has been measured up to a Reynolds number of 10^4. Sections 2, 3, and 4 are mainly reviews of results obtained with different configurations, while Section 5 shows preliminary results of a new study. The different types of oscillations produced by a tethered sphere are examined when the thread is parallel to the direction of the flow. Some overall conclusions are given in Section 6.

* Corresponding author.
E-mail address: Thomas Leweke@irphe.univ-mrs.fr (T. Leweke).

0997-7546/$ – see front matter
doi:10.1016/j.euromechflu.2003.09.007

For cylinders and spheres, the Reynolds number is based on the transverse diameter D, the mean upstream velocity U and the kinematic viscosity ν of the fluid: $Re = UD/\nu$. Wake frequencies f are expressed in the form Strouhal numbers, defined by $St = fD/U$.

2. The Landau model

The concepts of absolute and convective instabilities have been introduced in plasma physics [8] and applied later to shear flows (see the review by Huerre and Monkewitz [9]). The development of a global mode of wake oscillations has been associated to the existence of regions of absolute and convective instability behind the body, linked to the downstream evolution of the transverse velocity profile. The selection of the frequency is due to the feedback between upstream and downstream perturbations, when the size of the region of absolute instability is big enough to create a global mode. Non-linear effects and the saturation of this mode are well described by the Landau model. In his original paper, Hopf [10] underlined that "the bifurcation of a periodic solution from a stationary solution is observable ... for example, in the flow around a solid body". The approach developed by Landau [11] analyses the stability of a steady flow. A non-stationary perturbation of the steady solution of the Navier–Stokes equation is expanded as a sum of modes $A(t)g(\boldsymbol{x})$, where the spatial variation g is then omitted for the sake of simplicity. Let us consider a temporal mode $A(t)$ proportional to $\mathrm{e}^{\sigma t}$, with relative growth rate:

$$\sigma = \sigma_r + \mathrm{i}\sigma_i. \tag{1}$$

In the subcritical regime, $Re < Re_c$, all disturbances are stable and σ_r is negative. At the threshold of instability, when $Re = Re_c$, one normal mode is marginally stable, $\sigma_r = 0$, with two angular frequencies σ_i and $-\sigma_i$. As the Reynolds number is increased above the critical value, the coefficient σ_r becomes positive and, near the threshold of instability, it might be considered as a linear variation of the Reynolds number, i.e., proportional to $Re - Re_c$. The exponential growth of the amplitude is no longer valid for long times, and the Landau model takes into account a non-linear saturation in a new expression of the time derivative:

$$\frac{\mathrm{d}A}{\mathrm{d}t} = \sigma A - l\left|A^2\right|A, \tag{2}$$

where the complex coefficient of the non-linear term is $l = l_r + \mathrm{i}l_i = l_r(1 + \mathrm{i}c_2)$. Writing the complex amplitude $A = M\,\mathrm{e}^{\mathrm{i}\phi}$, the evolution equations for the modulus M and the phase ϕ are:

$$\frac{\mathrm{d}M}{\mathrm{d}t} = \sigma_r M - l_r M^3 \tag{3}$$

and

$$\frac{\mathrm{d}\phi}{\mathrm{d}t} = \sigma_i - l_i M^2. \tag{4}$$

This model is consistent with the temporal growth of a global mode resulting from a large absolutely unstable zone, without hysteresis when changing the Reynolds number, and with a temporal growth rate independent of the spatial location.

3. The cylinder configuration

3.1. The parallel mode and the Landau model

For the case of the cylinder, the bifurcation from steady to periodic flow occurs while breaking the transverse spatial symmetry ($y \to -y$), near a critical Reynolds number $Re_c \approx 47$ (see Fig. 1). y is the coordinate perpendicular to the flow direction x and the cylinder axis z. In this section, we neglect variations along the span of the cylinder, which, in experiments, corresponds to parallel vortex shedding requiring a careful control of the flow (see Williamson [12,13] and other authors [14, 15]), or to the configuration of a ring with periodic conditions (Leweke et al. [16]). The equation of the modulus (3) predicts the variation of the saturated energy of oscillation:

$$M_{\mathrm{eq}}^2 = \sigma_r / l_r \sim Re - Re_c. \tag{5}$$

Such a behaviour is clearly observed in the experimental result in Fig. 2. From many measurements and 2D numerical simulations, the value of the temporal growth rate has been deduced and is now well known:

$$\sigma_{r,\mathrm{cyl}} = 0.2(Re - Re_c)\frac{\nu}{D^2}. \tag{6}$$

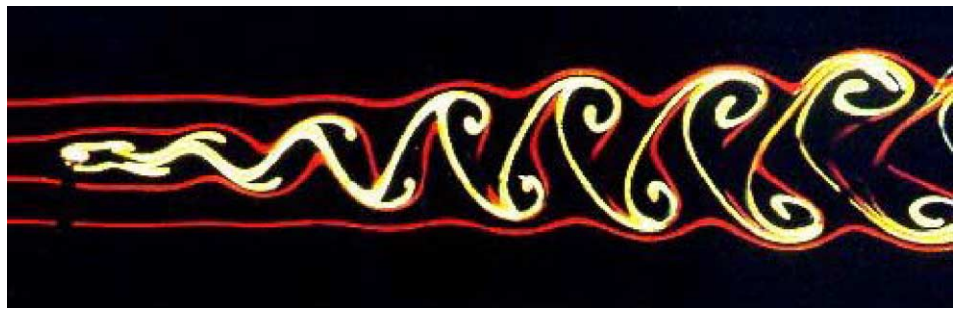

Fig. 1. Visualisation of the vortex shedding behind a circular cylinder at $Re = 65$.

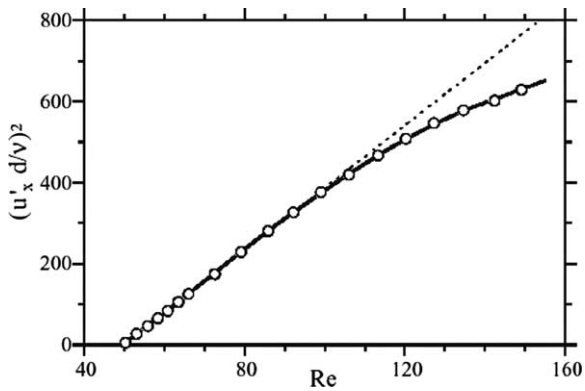

Fig. 2. Energy of the fluctuating streamwise velocity (u'_x) as function of the Reynolds number for the parallel shedding mode downstream of a torus (from [16]).

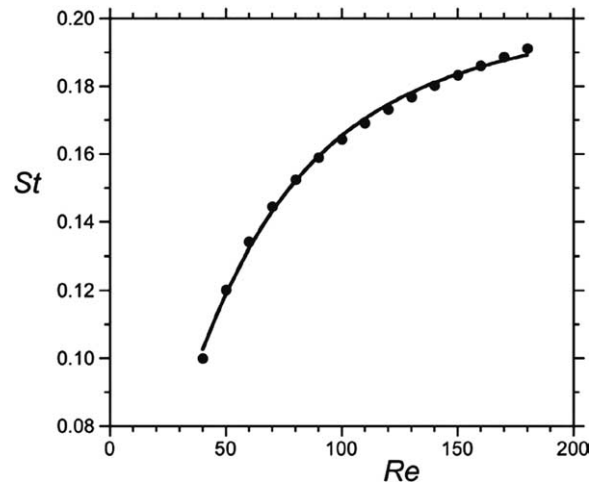

Fig. 3. *St–Re* relationship deduced from the Villermaux model (line) with $a = 123$, $b = 0.44$, $c = 1.1$ and experimental measurements for the parallel mode behind a torus (symbols from [16]).

An expansion of Eq. (4) governing the frequency leads to an expression for the Strouhal–Reynolds number dependence. There is a non-linear variation of the frequency with the amplitude M of the oscillation and the coefficient $c_{2,\mathrm{cyl}} = l_i/l_r = -3.0$ has been deduced from transient recordings [17,18]. In principle, this analysis should be restricted to a narrow range in Reynolds number near the bifurcation threshold where the Landau approximation is valid. However, the astonishing fact is the linear variation observed in Fig. 2 over a large range of Reynolds number, where the "small" parameter, $\varepsilon = (Re - Re_c)/Re_c$, reaches values as large as 3! The amplitude of oscillation varies along the streamwise direction from 0 in the vicinity of the solid boundary of the cylinder to a maximum and decreases in the far wake. This evolution is consistent with the description of global modes [19].

Villermaux [20] has proposed to consider two separate amplitudes A and B on each side of the vortex street, i.e., to describe the wake through two oscillators, driven by the shear U/D near the body, and interacting with a certain delay corresponding to the recirculation time $\tau = cD/U$:

$$\frac{\mathrm{d}A}{\mathrm{d}t} = s_r\big(1 - \big[A + \alpha B(t-\tau)\big]\big)A,$$
$$\frac{\mathrm{d}B}{\mathrm{d}t} = s_r\big(1 - \big[B + \alpha A(t-\tau)\big]\big)B. \tag{7}$$

The growth rate s_r, similar to σ_r in the Landau model, has the same dimension as the shear U/D, and the constant α has been introduced to model the coupling of the two non-linear oscillators A and B [20]. The oscillation occurs when the product $s_r\tau$ is larger than a critical value. One can then work out an expression for the Strouhal number of the wake, which depends on three non-dimensional constants a, b (functions of the shape of the velocity profile in the wake), and c, and on the Reynolds number (Fig. 3):

$$St = b/\big(bc + \big(1 + \big(a^2/Re^2\big)\big)^{1/2}\exp\big\{bc/\big[1 + (a/Re)^2\big]^{1/2}\big\}\big). \tag{8}$$

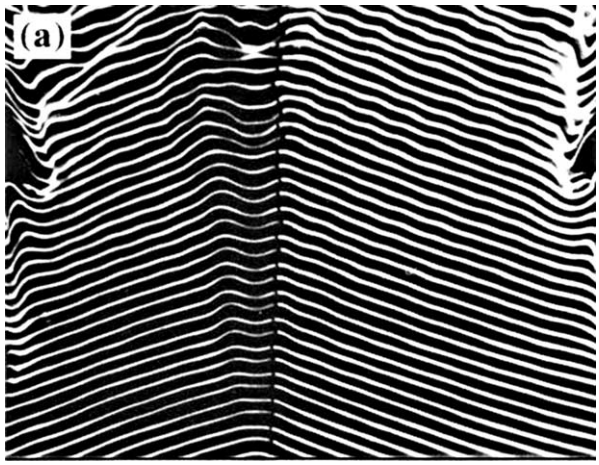

Fig. 4. Visualisation of "chevrons" behind a circular cylinder (from [13]).

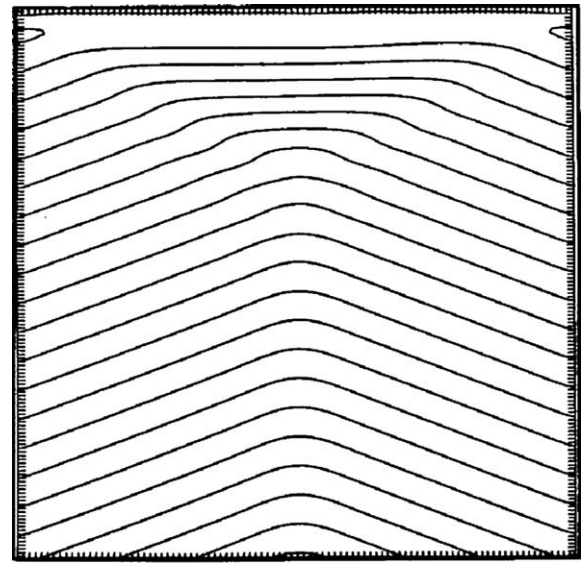

Fig. 5. Lines of constant phase of the Ginzburg–Landau equation (from [22]).

A least-squares fit of (8) to experimental results is shown in Fig. 3. The fitted parameter c has the value 1.1, which implies a recirculation zone of length $\sim 1D$, in agreement with observations of the flow.

3.2. Three-dimensional effects and the Ginzburg–Landau model

The Ginzburg–Landau model [21,22] is an extension of the Landau model by addition of a diffusive term along the spanwise direction.

$$\frac{\partial A}{\partial t} = (\sigma_r + \sigma_i)A - (l_r + \mathrm{i}l_i)\left|A^2\right|A + (\mu_r + \mathrm{i}\mu_i)\frac{\partial^2 A}{\partial z^2}. \tag{9}$$

It describes the three-dimensional phenomena (oblique shedding, cellular structure and dislocations, variation of the critical Reynolds number) observed in the wake of a finite circular cylinder as a collective interaction of non-linear oscillators. In this approach, the time evolution is essentially equivalent to the streamwise direction: $x = Ut$. Figs. 4 and 5 show a visualisation of a "chevron" pattern by Williamson [12] and the isophase lines of the Ginzburg–Landau model with zero conditions at the ends [22,23]. Dislocations and cellular structures are shown in Fig. 6 (a) and (b). The value of the diffusive term μ_r has been deduced from different measurements and is equal to roughly 10ν. The model predicts the variation of the critical Reynolds number as function of the aspect ratio L/D of the cylinder. Moreover, helical lines have been observed in the wake of a ring [16], and the Eckaus secondary instability has been successfully related to the oblique shedding from the end of a circular cylinder [24]. A similar modelling using diffusive van der Pol oscillators has been introduced by Gaster [25] and recently renewed by Fachinetti, de Langre and Biolley [26].

4. The sphere configuration

4.1. Bifurcation series

In contrast to the cylinder, for the sphere wake, there are two bifurcations leading to a time-dependent (periodic) flow [27]. Increasing the Reynolds number, a regular axisymmetry-breaking bifurcation occurs first, giving rise to a wake with a plane symmetry. Numerical simulation results presented by Thompson, Leweke and Provansal [28] have shown that the amplitude of the azimuthal mode is well described by a Landau model (3) with real coefficients l (Fig. 7), near the critical Reynolds number $Re_1 = 212$. The growth rate has been determined as

$$\sigma^1_{r,\mathrm{sphere}} = 0.6(Re - Re_1)\frac{\nu}{D^2} \tag{10}$$

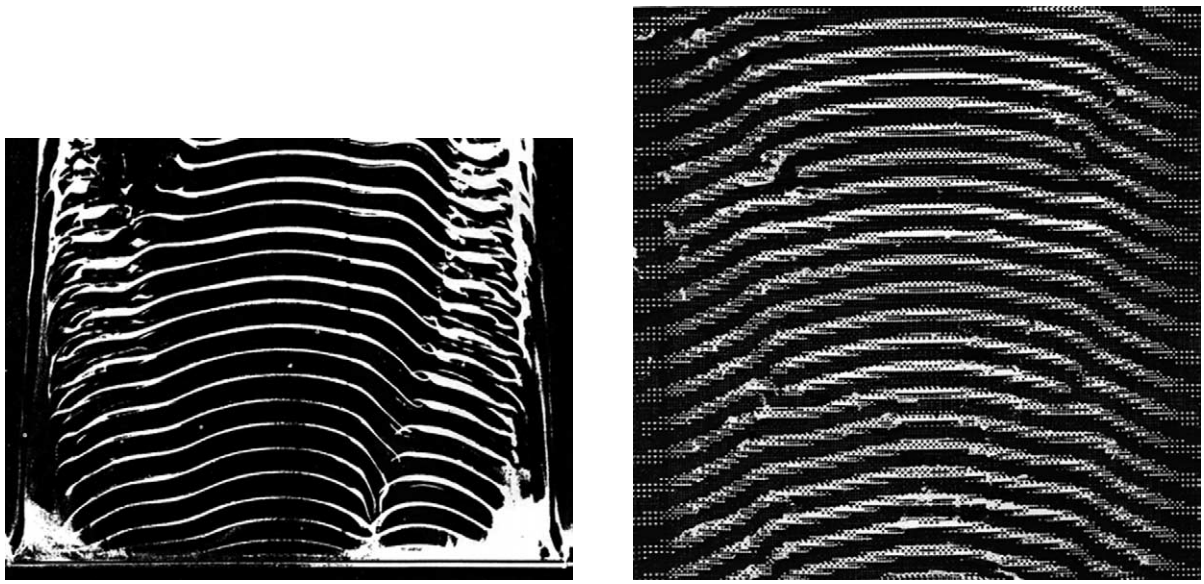

(a) (b)

Fig. 6. (a) End cells and dislocations behind a circular cylinder (from [13]). (b) Simulation of the Ginzburg–Landau model with a boundary layer (from [23]).

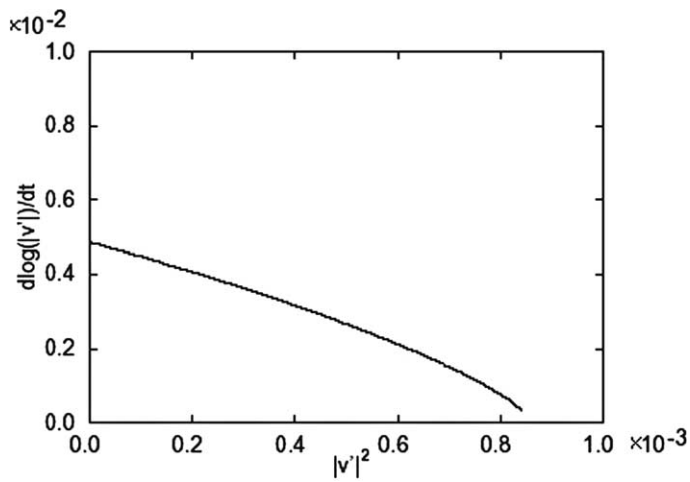

Fig. 7. Variation of growth rate with amplitude of the first bifurcation mode (break of axisymmetry) in the wake of a sphere (from numerical simulations reported in [28]).

as well as the value and the sign of l_r. In experiments, the sphere is rigidly held by a small pipe (Fig. 8), which allows the injection of dye through a small hole. The direction of the pipe, slightly inclined with respect to the flow direction in the vertical plane x–z, allows the selection of the orientation of the wake. The visualisations shown in Fig. 9 (a) and (b) show the stationary wake from two perpendicular view directions. Between $Re = 270$ and $Re = 280$, the transition to periodic flow appears for a higher critical Reynolds number Re_2. The periodic shedding of vortex loops has also been modelled by the complex Landau equation (3). Fig. 10 shows the experimental variation of the energy of oscillation measured at a given point. For the sphere, the linear part exists over a much smaller range of Reynolds numbers than in the case of the cylinder, $\varepsilon = (Re - Re_2)/Re_2 = 0.05$. The same measurements were made from numerical simulations by Thompson, Leweke and Provansal [28] and Ghidersa and Dušek [29]. A similar plot is obtained when measuring the maximum of fluctuating energy in the streamwise direction [30], as it should be when there exists a global mode [19]. The typical downstream evolution of the energy is plotted in Fig. 11.

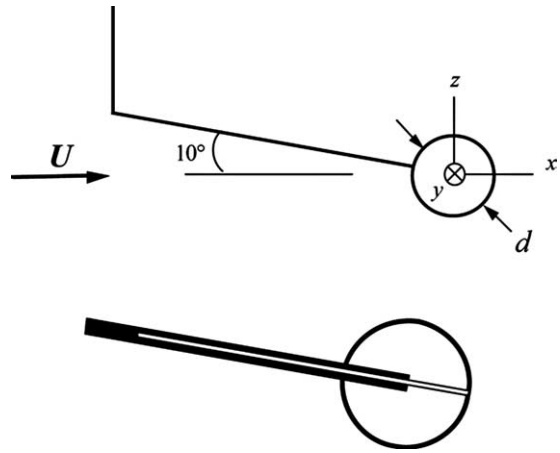

Fig. 8. Sketch of the rigidly held sphere and experimental details.

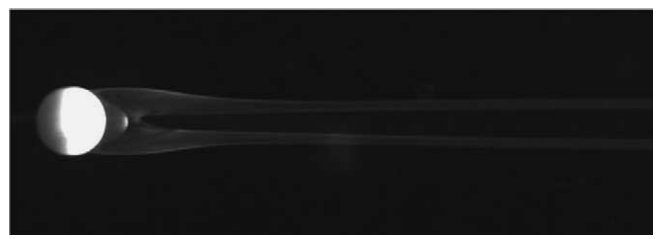

(a)

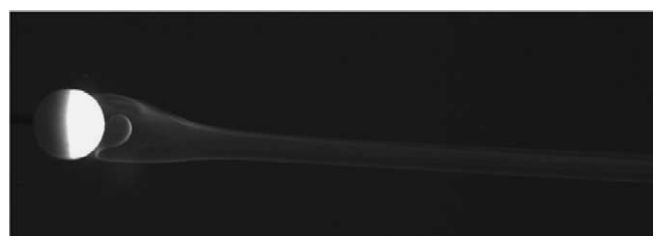

(b)

Fig. 9. Visualisation of the wake of a sphere at $Re = 270$: (a) top view, (b) side view in a plane containing the rigid support rod (from [27]).

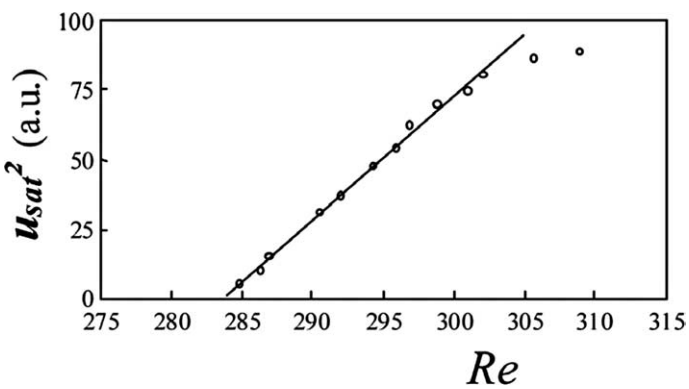

Fig. 10. Energy of the periodic streamwise velocity as function of the Reynolds number in the wake of a sphere, $D = 1.0$ cm (from [27]).

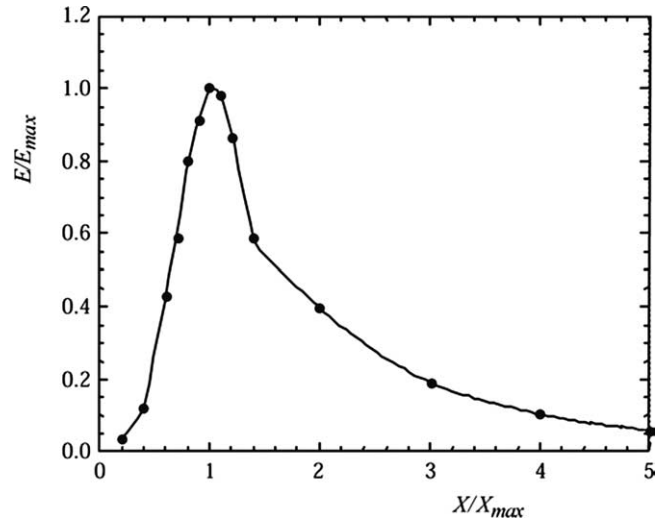

Fig. 11. Global mode variation downstream of the sphere (data from [30] normalised by the maximum in amplitude as in [10]).

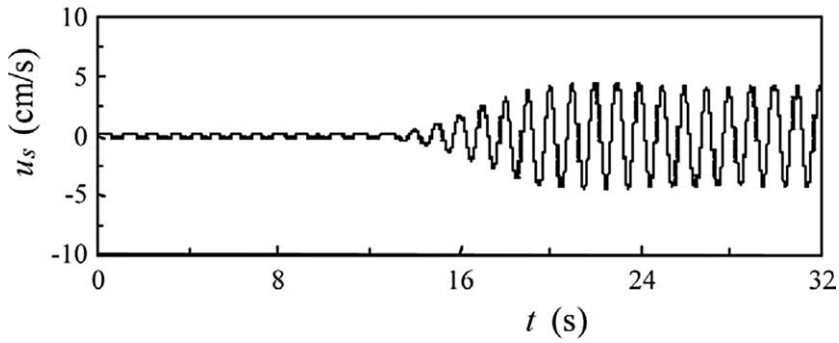

Fig. 12. Transient evolution of the amplitude of oscillation in the periodic regime of the sphere wake.

Transient regimes (Fig. 12, and see [27]) have been investigated in order to obtain the temporal growth rate for the second transition:

$$\sigma^2_{r,\text{sphere}} = 0.6(Re - Re_{cs})\frac{\nu}{D^2} \tag{11}$$

which, within the measurement accuracy, is identical to the one of the first transition in (10), and the influence of non-linear terms in amplitude upon the vortex shedding frequency (see Eq. (4)). The value of the critical Reynolds number deduced from experiments is $Re_{cs} = 283 \pm 6$ which is fairly close to the range [270, 280] obtained from various numerical simulations [28, 29,31–33]. In our experiments, a small transverse jet is used to destroy the wake during a short time and to analyse the growth of the global mode. The experimental value of the constant $c_{2,s}$ is found to vary from -0.7 to -0.1 when the Reynolds number changes from 290 to 320. From their numerical simulations, Thompson et al. [28] and Ghidersa and Dušek [29] calculate a value for $c_{2,s}$ of about -0.5. Therefore, for the sphere the absolute value of the constant $c_{2,s}$ appears to be lower than in the case of a cylinder. A weak value of $c_{2,s}$ means that a non-linear van der Pol oscillator might also be used for the wake of the sphere. For a short cylinder within wall-boundaries ($L/D = 5$), Peschard, Le Gal and Takeda [34] have obtained a value $c_{2,\text{cyl}} = -1.0 \pm 0.1$, for a Reynolds number of the order of 150, which is intermediate between the values of a long cylinder and of a sphere. Changing the Reynolds number in the range 50 to 300 and varying the shape of the bluff body both have an effect on the value of the non-linear coefficient c_2, it is not clear which of these effects is more important.

A major discrepancy appears between the visualisation of streaklines downstream of the sphere and the iso-surface plot of the vorticity structure deduced from numerical simulations. The location of injection of dye in experiments and the initial point of particles in numerical simulations might explain the difference of topology (see, e.g., the discussion about this point by Schouveiler et al. [35]). Two sides of a “vortex loop street”, with different signs of vorticity, are visible, which can be modelled again by two coupled oscillators. Thus, the model presented by Villermaux [20] for the cylinder still works in the case of a

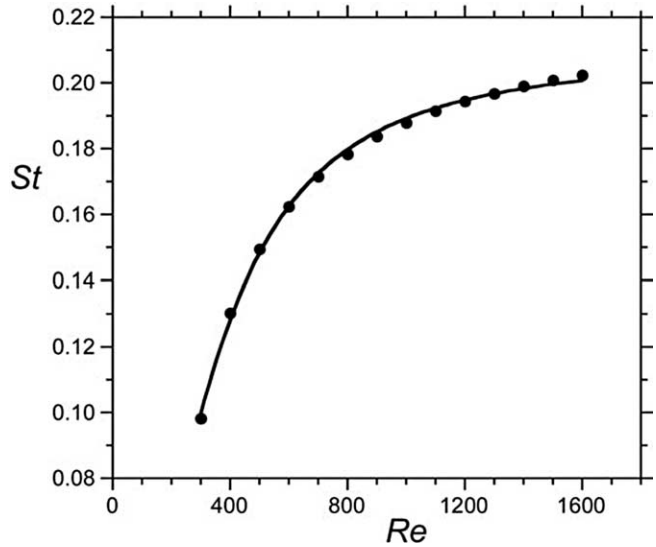

Fig. 13. *St–Re* relationship deduced from the Villermaux model (dashed line) for $a = 2500$, $b = 1.29$, $c = 1.33$, and experimental measurements behind a sphere (symbols).

sphere, with different values of parameters but the same scaling based upon the recirculation length in a large Reynolds number range (270–1500, see Fig. 13). We have explored the evolution of the Strouhal number with the Reynolds number, when varying the upstream velocity and the diameter of the sphere in a wind tunnel (Fig. 14). Sakamoto and Haniu [36,37] have reported the existence of two modes, high and low frequencies, for Reynolds number higher than 800. Here, the sphere is held by a rigid pipe and we have always observed the low frequency mode. In the laminar regime and the irregular range, the Strouhal number increases up to a value $St = 0.2$, which is the same as for the case of the cylinder. For Reynolds number of 3000, velocity signals are quite irregular and there is a large uncertainty in the determination of the frequency and Strouhal number: different experiments lead to different results for the same Reynolds number. In the Reynolds number range 3000–6000, the Strouhal number decreases sharply then increases slightly from 6000 to 12000. At $Re = 7000$, the velocity signals are more regular than for $Re = 3000$ and the temporal autocorrelation increases. A similar variation of the Strouhal number and of the irregular vortex shedding has also been reported by Sakamato and Haniu [36,37].

4.2. Transitions from the sphere to the cylinder configuration

Different paths allow the transit from the characteristic alternating vortex street behind a cylinder to the wake of a sphere: transformation of the geometry of a short cylinder [38], coupling of two or several spheres along the transverse direction [35, 39], variation of the shape of the cylinder (as the sinuous cylinder used by Owen, Szewczyk and Bearman [40]), or changing the aspect ratio of a torus as in the work of Sheard et al. [41].

In a previous study [38], we have investigated the periodic vortex shedding in the wake of circular cylinders with free hemispherical ends (Fig. 15(a)). The two control parameters of this flow are the Reynolds number $Re = UD/\nu$ and the aspect ratio L/D where L is the spanwise length. The geometry is varied from the case of the sphere, for which L/D is equal to 1, to the configuration of two-dimensional parallel shedding behind a circular cylinder (corresponding to $L/D = \infty$). First, the thresholds Re_c for the transition to unsteady flow have been determined by extrapolating to zero the linear evolution, with *Re*, of the square amplitude of the streamwise velocity fluctuations. As for cylinders confined between two end plates, the stability of the wake of free-end cylinders is strongly affected by the variation of the aspect ratio. In fact, the critical Reynolds number Re_c increases when the aspect ratio is reduced and this behaviour agrees with the critical length predicted by the Ginzburg–Landau model (Fig. 15(b)). The non-dimensional frequency, Strouhal number $St = fD/U$, is a function of the Reynolds number, and our measurements reveal a continuity between the cylinders ($L/D = 5$ to 2) and the case of the sphere ($L/D = 1$).

The case of uniform flow over a structure with a sinuous spanwise variation (Fig. 16) has been investigated by Owen, Szewczyk and Bearman [40]. Their visualisations indicate that the regular vortex shedding observed behind a uniform cylinder is suppressed: vortex loops similar to the shedding behind a sphere are observed (see Fig. 17). The comparison between the wake of a sphere or a short cylinder ($L/D = 2$) and the wavy cylinder used by Owen et al. [40] exhibits strong common features in the shape of vortex loops, as well as in the frequency laws. In recent experiments of our team, the amplitude and

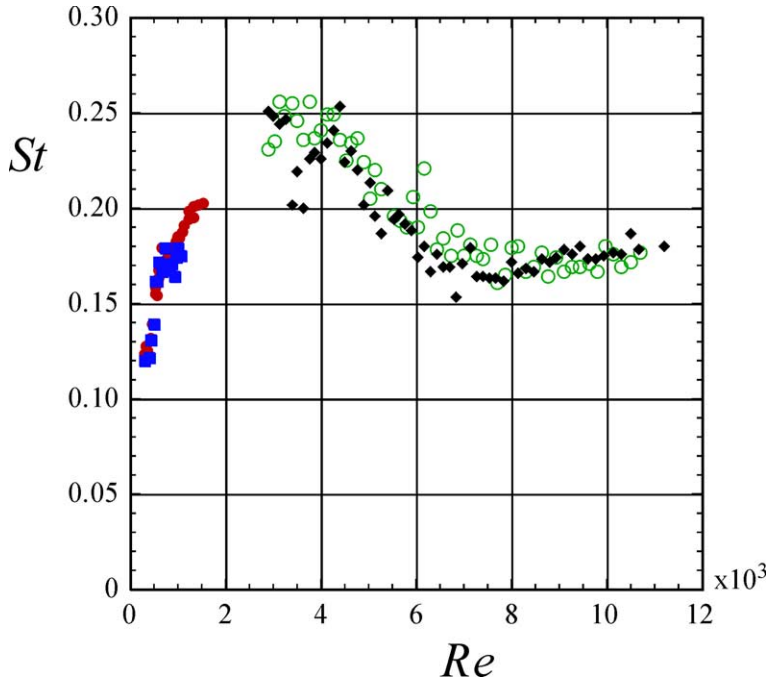

(a)

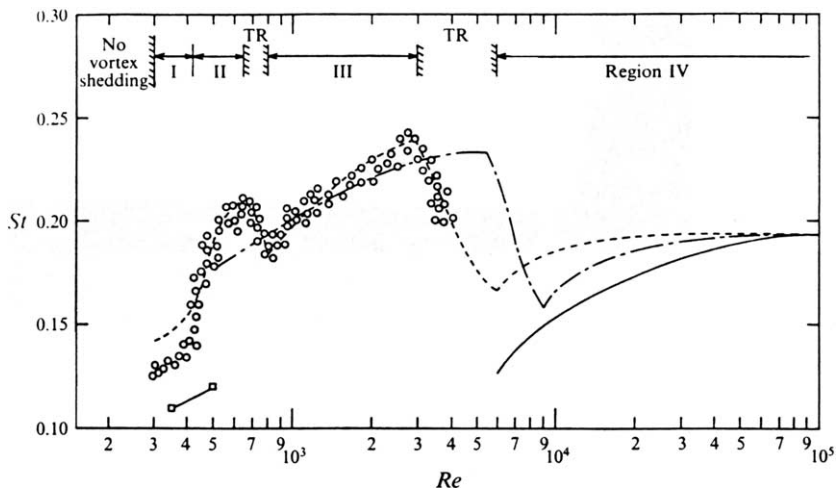

(b)

Fig. 14. (a) Hot wire measurements of *St* vs. *Re*, made 5 diameters downstream of spheres of different diameters ($D = 1.0$, 3.9, 6.4 cm), over a large Reynolds number range. (b) Data from Sakamoto and Haniu [23].

frequencies along the spanwise direction were measured. The amplitude has a nonzero value only in separate cells where the vortex shedding is similar to the shedding behind a sphere.

Another possibility is to study the interaction of two spheres along the transverse direction. When the distance h between the centres of the spheres is much larger than D, each sphere acts as an isolated sphere. When the two spheres are in contact ($h/D = 1$), the geometry is very close to the one of a short cylinder of aspect ratio $L/D = 2$, and the interaction of vortex loops lead to a pattern similar to the alternating vortex street behind a circular cylinder. A detailed investigation of this transition is reported in this issue by Schouveiler et al. [35].

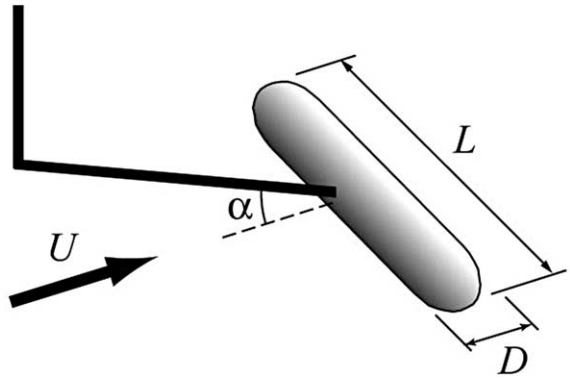

(a)

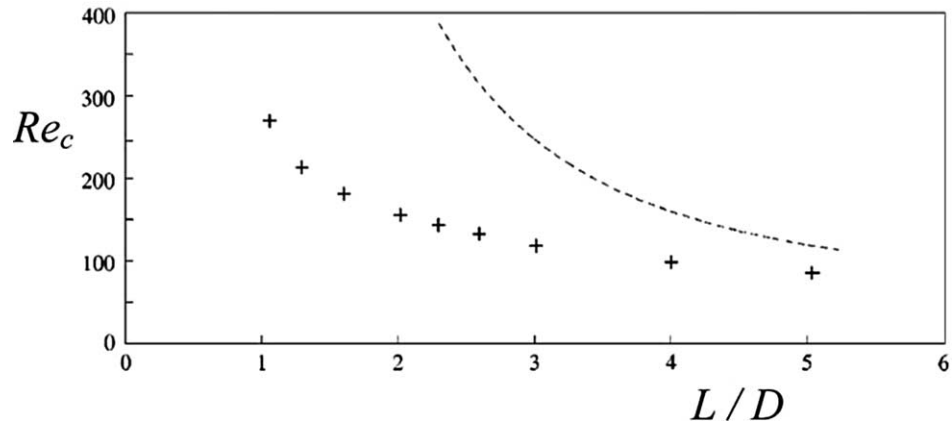

(b)

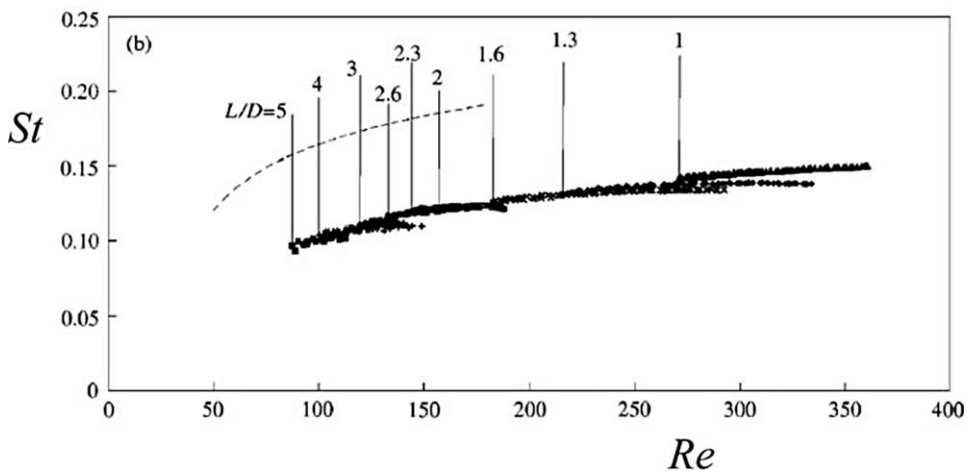

(c)

Fig. 15. (a) Sketch of a short cylinder with hemispherical ends. (b) Variation of the critical Reynolds number with aspect ratio; dashed line: cylinder between end plates. (c) Strouhal number versus Reynolds number curves for cylinders of different aspect-ratios; dashed line: parallel shedding behind an infinite cylinder (from [38]).

In special cases, the wake of a single sphere can be quite similar to the two-dimensional wake of a circular cylinder. Such a situation occurs when three-dimensional effects are frozen in the transverse direction as in the case of a sphere immersed in a

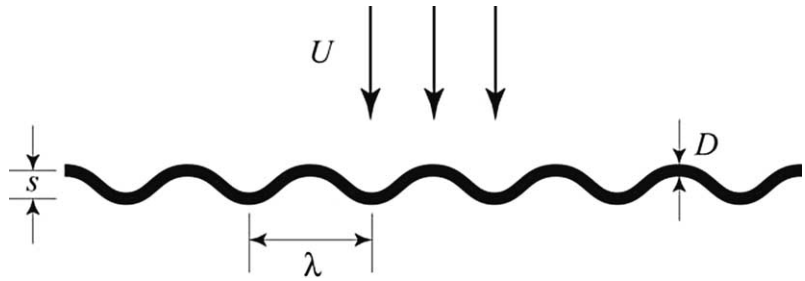

Fig. 16. Geometry of the sinuous cylinder.

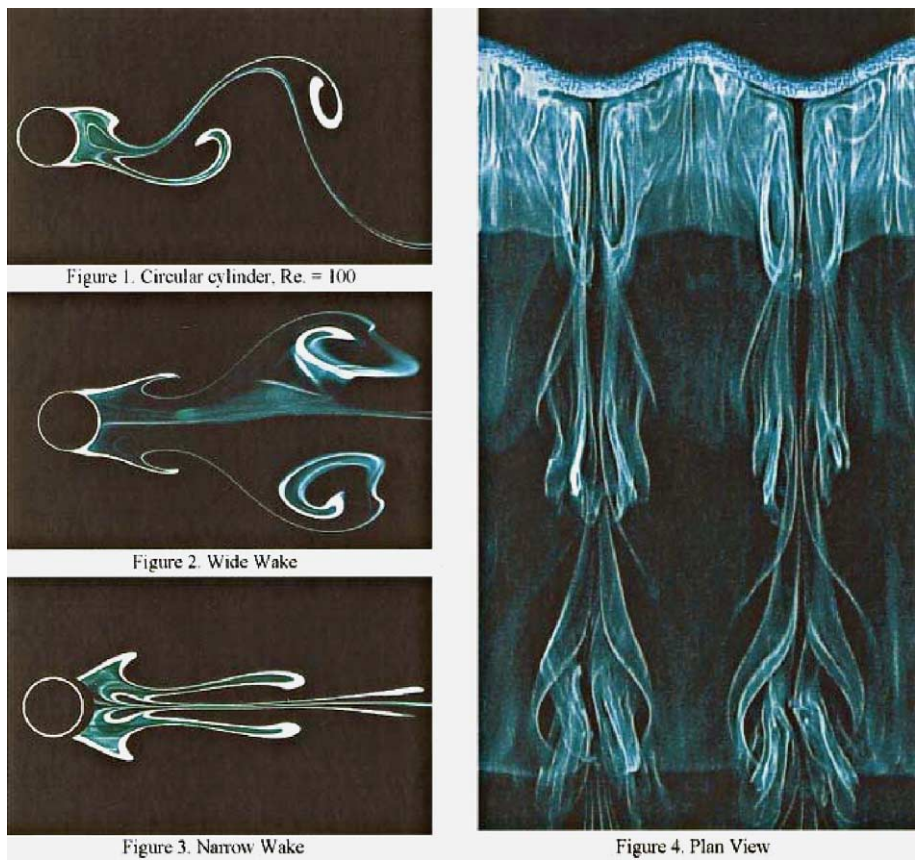

Fig. 17. Visualisations from Owen, Szewczyk and Bearman [40] of the wake downstream of a sinuous cylinder.

stratified flow (see Berger and Wille [42]), or of a sphere in a moving soap-film (for instance the experiment similar to the work performed by Gharib and Derango [43] or Couder, Chomaz and Rabaud [44] with a sphere instead of a cylinder).

5. Dynamics of a tethered sphere

5.1. Motivations of the study

The vibration of a tethered sphere in a uniform stream is an example of fluid–structure interaction similar to the vibration of a flexible cylinder. In our case, following the terminology used by the group of Williamson [45,46], the reduced parameters of this system are the relative density or mass ratio, m^*, which is equal to the ratio of the mass of the sphere to the displaced fluid mass, and the reduced velocity $U^* = U/f_n D$, based on the velocity U of the free stream, the diameter D of the sphere, and the

natural frequency of the system f_n. The natural frequency of the tethered sphere varies with the length of the pendulum L' and the gravity g' as

$$f_n = \frac{1}{2\pi}\sqrt{\frac{g'}{L'}}. \tag{12}$$

Here, the gravity g' is modified by the influence of buoyancy force and by the change in the inertia due to the added mass, which is usually equal to 0.5 times the mass of the fluid displaced by the sphere, in such a way that

$$g' = \frac{m^* - 1}{m^* + 0.5}g, \tag{13}$$

where g is the standard gravitational acceleration. At low reduced velocity ($U^* < 1$), the sphere is at rest and, increasing the velocity of the flow, the sphere begins to oscillate above a critical value U_c^*. The configuration of a thread transverse to the flow has been thoroughly examined by Jauvtis, Govardhan and Williamson [45]. In this case, the gravity induces a particular direction in the transverse plane; therefore the oscillations of the sphere induced by the vortex shedding and the time-periodic lift are mainly in-line along the transverse horizontal direction. Different modes appear when varying the relative density ratio and the reduced velocity. We have chosen to examine a case where the thread holding the sphere is initially parallel to the direction of the upstream flow. To our knowledge, there is no result available for this configuration. As the gravity is aligned with the direction the flow, all the transverse directions are equivalent and different oscillation patterns may occur.

5.2. Results

These experiments have been conducted in a vertical water channel with a circular test section of diameter 8 cm and of length 100 cm. The current in the channel is created by gravity. The sphere, made of glass of density $\rho_{\text{sphere}} = 2430\ \text{kg/m}^3$ and of diameter $D = 16.6$ mm, is attached with glue to a thread supported by a small horizontal metal pipe (see Fig. 18). The velocity of the flow is deduced from flow-rate measurement, after corrections taking into account the development of boundary layers along the wall of the channel and the blockage effect due to the sphere. The length L' of the thread has been varied from 15 to 35 cm. A mirror has been positioned behind the channel with an angle of 45° to the front direction in order to two perpendicular views get on the same image. Details of the experimental set-up and of the image processing method are described in [47]. The reduced velocity is limited to a narrow range from 0 to 5 with this channel and this sphere. The diameter of the sphere is

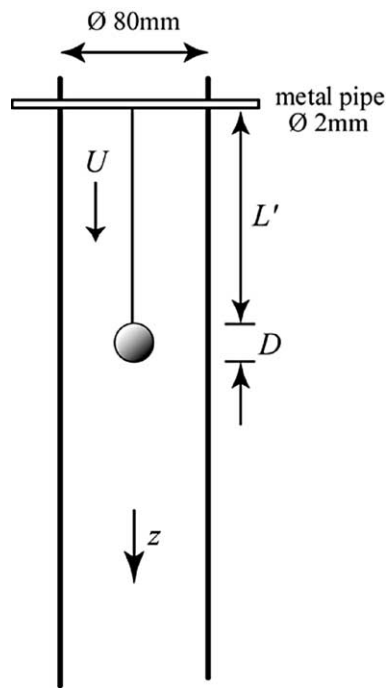

Fig. 18. Sketch of the experimental set-up for the study of flow around a tethered sphere.

the largest possible without boundary or wall effects on the movement of the sphere. The Reynolds number was in the range 600–800 for this series of measurements.

Oscillations occur when the reduced velocity is greater than a critical value U_c. The period of oscillation has been directly measured and also deduced from video recordings and image processing. In our measurements, the frequency f of oscillation is always locked to the natural frequency f_n of the suspended sphere, given by relation (12), and Fig. 19(a) shows a reduced frequency $f^* = f/f_n$ fairly close to 1. The trajectories of the sphere, in the horizontal plane x–y, have been deduced from the sequence of two perpendicular views. Depending on initial conditions, elliptic, quasi-circular, or even straight (planar) oscillations may occur. The planar oscillations are unstable; they were observed in transient regimes, leading eventually to circular or elliptic trajectories. In the context of two-phase flows, different authors [48,49] have reported observations of similar oscillations of bubbles in a plane or along helical paths. The present case of a tethered sphere represents a simplified model of such flows with fewer degrees of freedom. Moreover, it appears that the amplitude, or peak-to-peak displacements, of linear

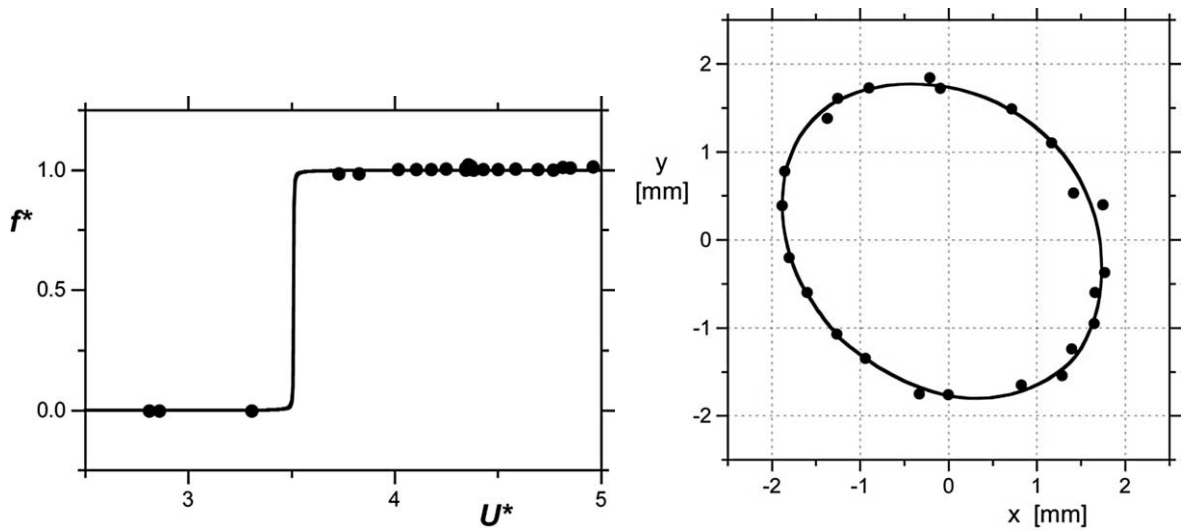

(a) (b)

Fig. 19. (a) Reduced frequency as function of the reduced velocity for a tethered sphere near the threshold. $L'/D = 9$. (b) Trajectory of the sphere in a plane transverse to the flow for $L'/D = 9$ and $U^* \approx 4$.

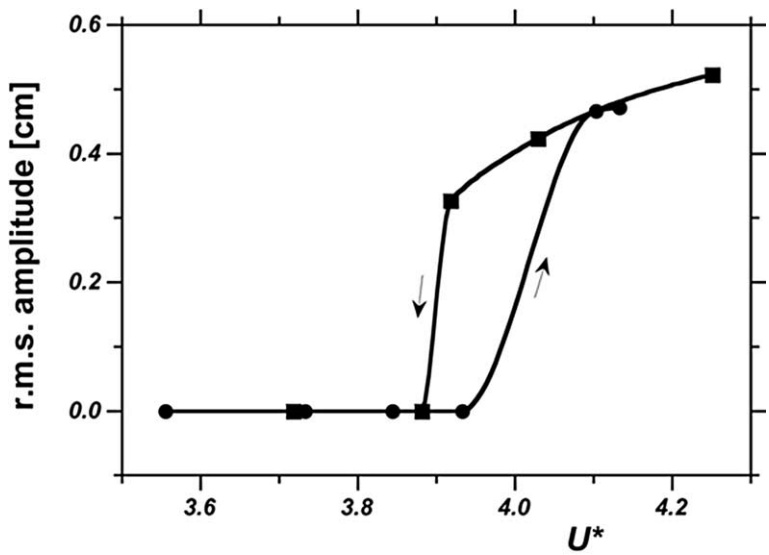

Fig. 20. Hysteresis of the threshold when varying reduced velocity. Tether length: $L'/D = 9$.

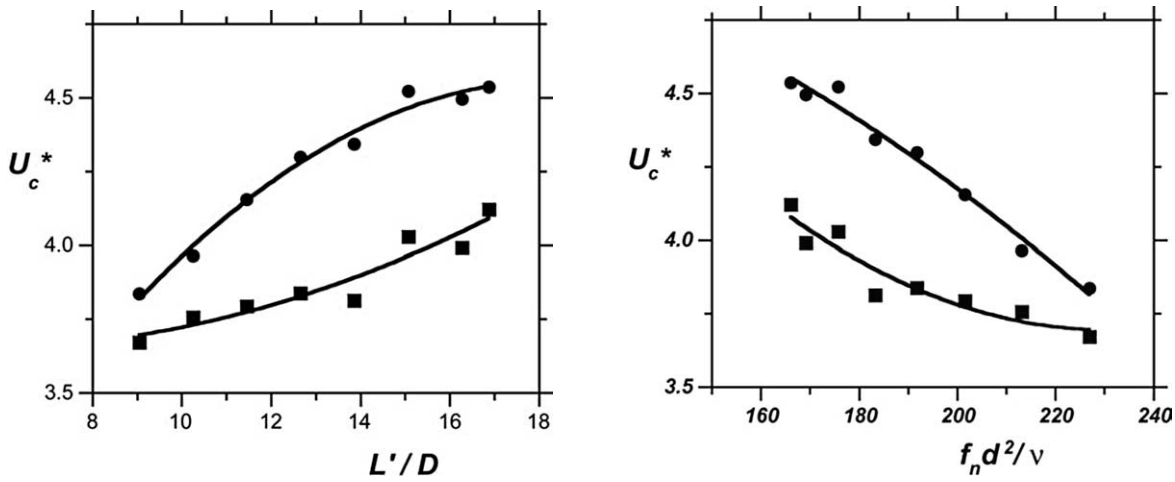

(a) (b)

Fig. 21. Critical reduced velocities defining the hysteresis, as function of (a) the tether length, and (b) the non-dimensional natural frequency.

oscillations are greater than their values for elliptic or circular modes. A typical elliptic record is shown on Fig. 19(b): the orientation of the major and minor axes of the ellipse is unknown before a given experiment and is not necessarily aligned with the front and perpendicular views determined by the location of the mirror. The amplitude of oscillation defined by $(A_1^2 + A_2^2)^{1/2}$, where A_1 and A_2 are the peak-to-peak values of movement along the major and minor axes, has been measured as function of the reduced velocity. When decreasing the velocity of the flow, the phenomenon of oscillation disappears at a value of the reduced velocity which is lower than the one where it appears when increasing U^* (Fig. 20). This hysteresis in the onset of oscillations is found for a whole range of tether lengths. Fig. 21 shows, how the two critical reduced velocities vary with the tether length or, alternatively, with the natural frequency. This phenomenon appears also in the case of the vortex induced vibrations of a cylinder. It has furnished a criterion to Facchinetti, de Langre and Biolley [50] for the selection of a phenomenological model and the definition of the coupling between the near wake and the solid structure of the bluff-body.

6. Conclusion and perspectives

Among bluff bodies wakes, the configurations of the circular cylinder and the sphere present different kinds of symmetry. Their applications concern various domains such as flow rate measurements, heat transfer behind a row of circular cylinders in heat exchangers, two-phase flows, and the dynamics of drops and bubbles. The experimental features of the first steps in the transition to turbulence have been described and clarified through the comparison to phenomenological models. The real and complex Landau models allow a description of the steady non symmetric amplitude of the sphere wake, as well as of the periodic regimes of both the sphere and cylinder. The non-linear behaviour of amplitude and frequency has also been deduced from streamwise velocity fluctuations measurements. Three-dimensional effects of real wakes behind low-aspect ratio cylinders are also well described by the diffusive coupling of oscillators along the span, as in the Ginzburg–Landau model or for coupled van der Pol oscillators.

The development of various three-dimensional numerical simulations is now a powerful tool to investigate the transition from the sphere to the circular cylinder wake. In this paper, we have mainly paid attention to the circular cylinder. However, we believe that the model is still working for any shape such as square, rectangular or triangular cross section, and even the case of a flat rectangular plate perpendicular to the flow. It would be worthwhile to investigate how the characteristic parameters such as the growth rate, the critical Reynolds number, and the Landau constant, vary as function of these different geometries.

Besides the case of a sphere held by a small pipe, the oscillations of a tethered sphere have been investigated. Preliminary results have been obtained for the case of a tether parallel to the flow. The oscillations of the sphere are always locked to the natural frequency of the system. It would be useful to work on a larger reduced velocity range. The hysteresis observed in the transition might be described by some theoretical modelling of the fluid structure coupling through the position and the velocity or the acceleration of the end of the tether. The neutrally buoyant sphere is a specific case in which the natural frequency goes to zero. It will be useful to link the drag and lift coefficients of the wakes to the oscillations of the sphere and to determine the values of the main parameters where different behaviours can exist. An experimental study of this problem is currently underway.

References

[1] H. Bénard, Formation de centres de giration à l'arrière d'un obstacle en mouvement, C. R. Acad. Sci. Paris 147 (1908) 839–842.
[2] T. von Kármán, Über den Mechanismus des Widerstandes, den ein bewegter Körper in einer Flüssigkeit erfährt, Göttingen Nachr. Math.-Phys. Kl. (1911) 509–519.
[3] P.W. Bearman, Vortex shedding from oscillating bluff bodies, Annu. Rev. Fluid Mech. 16 (1984) 195–222.
[4] H. Eckelmann, J.M.R. Graham, P. Huerre, P.A. Monkewitz (Eds.), Bluff Body Wakes, Dynamics and Instabilities, Springer-Verlag, Berlin, 1992.
[5] T. Leweke, P.W. Bearman, C.H.K. Williamson (Eds.), Bluff Body Wakes and Vortex Induced Vibrations, J. Fluids Structures 15 (3/4) (2001).
[6] C.H.K. Williamson, Vortex dynamics in the cylinder wake, Annu. Rev. Fluid Mech. 28 (1996) 477–539.
[7] M. Zdravkovich, Flow Around Circular Cylinders, Oxford Science, 2002.
[8] A. Bers, Space–time evolution of plasma instabilities – absolute and convective, in: M.N. Rosenbluth, R.Z. Sagdeev (Eds.), Handbook of Plasma Physics, Vol. 1: Basic Plasma Physics, North-Holland, Amsterdam, 1983, pp. 451–517.
[9] P. Huerre, P.A. Monkewitz, Local and global instabilities in spatially developing flows, Annu. Rev. Fluid Mech. 22 (1990) 473–537.
[10] E. Hopf, Abzweigung einer periodischen Lösung von einer stationären Lösung eines Differentialsystems, Ber. Math.-Phys. Kl. Sächs. Akad. Wiss. Leipzig 94 (1942) 1–22; English translation: J.E. Marsden, M. McCracken (Eds.), The Hopf Bifurcation and its Applications, Springer, New York, 1976, pp. 163–193.
[11] L.D. Landau, On the problem of turbulence, Dokl. Akad. Nauk. SSR 44 (1944) 339–342; English translation: D. ter Haar (Ed.), Collected Papers of L.D. Landau, Gordon and Breach, New York, 1965, pp. 387–391.
[12] C.H.K. Williamson, Defining a universal and continuous Strouhal–Reynolds number relationship for the laminar vortex shedding of a circular cylinder, Phys. Fluids 31 (1988) 2742–2744.
[13] C.H.K. Williamson, Oblique and parallel modes of vortex shedding in the wake of a circular cylinder at low Reynolds numbers, J. Fluid Mech. 206 (1989) 579–627.
[14] M. Hammache, M. Gharib, An experimental study of the parallel and oblique vortex shedding from circular cylinders, J. Fluid Mech. 232 (1991) 567–590.
[15] H. Eisenlohr, H. Eckelmann, Vortex splitting and its consequences in the vortex street wake of cylinders at low Reynolds numbers, Phys. Fluids A 1 (1989) 189–192.
[16] T. Leweke, M. Provansal, The flow behind rings: bluff body wakes without end effects, J. Fluid Mech. 288 (1995) 265–310.
[17] M. Provansal, C. Mathis, L. Boyer, Bénard–von Kármán instability: transient and forced regimes, J. Fluid Mech. 182 (1987) 1–22.
[18] M. Schumm, E. Berger, P.A. Monkewitz, Self-excited oscillations in the wake of two-dimensional bluff bodies and their control, J. Fluid Mech. 271 (1994) 17–53.
[19] J.E. Wesfreid, S. Goujon-Durand, B.J.A. Zielinska, Global mode behaviour of the streamwise velocity in wakes, J. Phys. II Paris 6 (1995) 1343–1357.
[20] E. Villermaux, On the Strouhal–Reynolds dependence in the Bénard–Kármán problem, in: T. Leweke, P.W. Bearman, C.H.K. Williamson (Eds.), Book of Abstracts – IUTAM Symposium on Bluff Body Wakes and Vortex-Induced Vibrations, Marseille, France, 2000.
[21] W. van Saarloos, Front propagation into unstable states, Phys. Rev. (2003), submitted for publication.
[22] P. Albarède, M. Provansal, Quasi-periodic cylinder wakes and the Ginzburg–Landau mode, J. Fluid Mech. 291 (1995) 191–222.
[23] P. Albarède, Self-organisation in the 3D wakes of bluff bodies, Ph.D. Dissertation, Université de Provence, Marseille, France, 1991.
[24] T. Leweke, M. Provansal, G.D. Miller, C.H.K. Williamson, Cell formation in cylinder wakes at low Reynolds numbers, Phys. Rev. Lett. 78 (1997) 1259–1262.
[25] M. Gaster, Vortex shedding from slender cones at low Reynolds numbers, J. Fluid Mech. 38 (1969) 565–576.
[26] M.L. Facchinetti, E. de Langre, F. Biolley, Vortex shedding modeling using diffusive van der Pol oscillators, C. R. Mécanique 330 (2002) 451–456.
[27] L. Schouveiler, M. Provansal, Self-sustained oscillations in the wake of a sphere, Phys. Fluids 14 (2002) 3846–3854.
[28] M.C. Thompson, T. Leweke, M. Provansal, Kinematics and dynamics of sphere wake transition, J. Fluids Structures 15 (2001) 575–585.
[29] B. Ghidersa, J. Dušek, Breaking of axisymmetry and onset of unsteadiness in the wake of a sphere, J. Fluid Mech. 423 (2000) 33–69.
[30] D. Ormières, M. Provansal, Transition to turbulence in the wake of a sphere, Phys. Rev. Lett. 83 (1999) 80–83.
[31] A.G. Tomboulides, S.A. Orszag, Numerical investigation of transitional and weak turbulent flow past a sphere, J. Fluid Mech. 416 (2000) 45–73.
[32] R. Natarajan, A. Acrivos, The instability of the steady flow past spheres and disks, J. Fluid Mech. 254 (1993) 323–344.
[33] T.A. Johnson, V.C. Patel, Flow past a sphere up to a Reynolds number of 300, J. Fluid Mech. 378 (1999) 19–70.
[34] I. Peschard, P. Le Gal, Y. Takeda, On the spatio–temporal structure of cylinder wakes, Exp. Fluids 26 (1999) 188–196.
[35] L. Schouveiler, A. Brydon, T. Leweke, M.C. Thompson, Interactions of the wakes of two spheres placed side by side, Eur. J. Mech. B Fluids 22 (2003), this volume.
[36] H. Sakamoto, H. Haniu, A study on vortex shedding frequency from spheres in a uniform flow, Trans. ASME J. Fluids Engrg. 112 (1990) 386–392.
[37] H. Sakamoto, H. Haniu, The formation mechanism and shedding frequency of vortices from a sphere in uniform shear flow, J. Fluid Mech. 287 (1995) 151–171.
[38] L. Schouveiler, M. Provansal, Periodic wakes of low aspect ratio cylinders with free hemispherical ends, J. Fluids Structures 15 (2001) 565–573.

[39] L. Schouveiler, M. Provansal, T. Leweke, Etude des sillages périodiques d'une ou de deux sphères et de cylindres droits ou ondulés à bouts libres, in: M. Ledoux (Ed.), Actes du 9e Colloque Francophone de Visualisations et de Traitement d'images en Mécanique des Fluides, Rouen, France, 2001, pp. 223–228.
[40] J.C. Owen, A.A. Szewczyk, P.W. Bearman, Suppression of Kármán vortex shedding, Phys. Fluids 12 (2000) S9.
[41] G.J. Sheard, M.C. Thompson, K. Hourigan, From spheres to circular cylinders: the stability and flow structures of bluff ring wakes, J. Fluid Mech. 492 (2003) 147–180.
[42] E. Berger, R. Wille, Periodic flow phenomena, Annu. Rev. Fluid Mech. 4 (1972) 313–340.
[43] M. Gharib, P. Derango, A liquid film (soap film) tunnel to study two-dimensional laminar and turbulent shear flows, Physica D 37 (1989) 406–416.
[44] Y. Couder, J.M. Chomaz, M. Rabaud, On the hydrodynamics of soap films, Physica D 37 (1989) 384–405.
[45] N. Jauvtis, R. Govardhan, C.H.K. Williamson, Multiple modes of vortex-induced vibration of a sphere, J. Fluids Structures 15 (2001) 555–563.
[46] A. Khalak, C.H.K. Williamson, Fluid forces and dynamics of a hydroelastic structure with very low mass and damping, J. Fluids Structures 11 (1997) 973–982.
[47] M. Provansal, T. Leweke, L. Schouveiler, N. Guébert, 3D oscillations and vortex induced vibrations of a tethered sphere in a flow parallel to the thread, in: Proc. of the 4th Pacific Symposium on Flow Visualization and Image Processing, Chamonix, France, 2003.
[48] M. Wu, M. Gharib, Experimental studies on the shape and path of small air bubbles rising in clean water, Phys. Fluids 14 (2002) L49–L52.
[49] G. Mougin, J. Magnaudet, Path instability of a rising bubble, Phys. Rev. Lett. 88 (2002) 014502.
[50] M.L. Facchinetti, E. de Langre, F. Biolley, On wake oscillator models for 2-D vortex-induced vibrations, J. Fluids Structures (2003), submitted for publication.